





**Observation of Le Sage gravity analog in complex plasma**

Andrey V. Zobnin <sup>\*</sup>, Andrey M. Lipaev <sup>†</sup>, Roman A. Syrovatka, Alexandr D. Usachev,  
Vadim N. Naumkin, and Oleg F. Petrov   
*Joint Institute for High Temperatures RAS, Moscow, 125412, Russia*

Markus H. Thoma   
*I. Physikalisches Institut, Justus-Liebig-Universität, Gießen, 35392, Germany*

Oleg V. Novitsky and Sergey N. Ryzhikov  
*Gagarin Research and Test Cosmonaut Training Center, Star City, 141160 Russia*



(Received 24 June 2024; accepted 20 August 2024; published 9 September 2024)

Fragmentation of a suspension of micron-sized plastic microparticles and their contraction into dense globules was experimentally obtained in a gas discharge plasma, when the plasma density was deliberately and abruptly increased. The globules took up spherical shapes 0.14–1.1 mm in diameters and contained from tens to thousands microparticles. The fragmentation and globule formation appears to be similar to the development of gravitational instability. This process is attributed to the Le Sage’s like attraction among microparticles in a dense plasma due to the plasma losses inside a globule hypothesized theoretically in the middle of the 1990s. The key role of plasma flows in the attraction was prominently demonstrated in the same experiment by the distinctly visible disintegration of the globules when we reduced the density of the surrounding plasma to the initial one. Also molecular dynamics simulations of fragmentation of microparticle clouds and globules formation qualitatively resemble typical patterns of the fragmentation and collapse of interstellar nebulae.

DOI: [10.1103/PhysRevE.110.035203](https://doi.org/10.1103/PhysRevE.110.035203)

**I. INTRODUCTION**

Dusty plasmas are ionized gases containing microparticles (“dust grains”). They can be found in the Universe, e.g., in comet tails, in planetary rings, on the lunar surface and in interstellar molecular clouds, as well as in plasma reactors for technical applications like etching and in fusion reactors. In laboratory experiments microparticles of a definite size are injected into a low-temperature plasma, produced by dc or rf discharges in a plasma chamber often containing noble gases. Those dusty plasma are sometimes called complex plasmas. The microparticles are usually negatively charged since they collect more electrons than ions on their surface due to the higher mobility of the electrons. The microparticle charges  $Q$  are in the range between  $10^3$  and  $10^5$  elementary charges depending on the size of the microparticles. Therefore the microparticles are able to build a strongly coupled many-body system. The structure and dynamics of the microparticle clouds can be directly observed by laser illumination and recoding by cameras on the microscopic level (individual particles) in real time. Hence complex plasmas are ideal model systems for studying the behavior of many-body systems, e.g., structure formation or phase transitions in equilibrium and nonequilibrium [1–3]. A famous example is the discovery of the plasma crystal in 1994 initializing a comprehensive

investigation of complex plasmas [4–7]. Since the microparticles are strongly affected by gravity, experiments with complex plasmas are also performed in microgravity. Since 2001 experiment facilities for the investigation of complex plasmas are operated on board the International Space Station (ISS) [8]. The present facility “Plasmakristall-4” (PK-4) was launched to the ISS in 2014 [9].

Usually, microparticles collect charges of the same sign and naturally repel each other. This short-range force is usually described by a screened Coulomb potential [10,11]. But interaction of microparticles with ambient neutrals and/or plasma can cause attraction between the microparticles under specific conditions. The possibility of attraction between charged particles of the same sign due to plasma fluxes was first predicted by Alexander Ignatov [12]. Ignatov’s idea is based on the mechanistic gravitation theory of 1748 by Georges-Louis Le Sage and was first proposed by Nicolas Fatio de Duillier in 1690. The theory underwent many revisions and corrections during the Age of Enlightenment and draw the attention of many great scientists, e.g., Leonhard Euler, Daniel Bernoulli, Immanuel Kant, Pierre-Simon Laplace, Lord Kelvin, James Clerk Maxwell, Hendrik Lorentz, J. J. Thomson, Henri Poincaré, etc. The theory relies on the concept of corpuscles that stream isotropically through the Universe and interact with massive bodies in a way similar to photons of electromagnetic radiation. Massive bodies cause some local deviation of isotropy in the stream of these corpuscles and produce an effect very similar to shadowing and, as a consequence, mutual attraction of the bodies. Although

<sup>\*</sup>Contact author: zobnin@ihed.ras.ru

<sup>†</sup>Contact author: lipaev@ihed.ras.ru

the theory has some flaws, it correctly confirms inverse proportionality to the square of distance between massive bodies, and in a later version, direct proportionality to their masses. Le Sage's theory almost directly fits to the case of a complex plasma, where microparticles suspended in the plasma play the role of massive bodies, and corpuscles have been replaced by ions. Ignatov's paper started a number of new theories which considered different nature of microparticles attraction [13–20]. Some of those approaches assume electrostatic interaction with nonlinear and nonequilibrium screening as a cause of attraction [15–17]. But in the papers [20–22] it was shown that in the electron-ion plasmas such attraction mechanisms can work only for positively charged microparticles. Thus, in a case of negatively charged microparticles the attraction can appear only due to drag forces, as a result of ion or neutral fluxes on the particles. This attraction could lead to formation of dense globules from dusty molecular clouds, which can considerably enhance the rate of gravitational collapse [23].

The effect of clustering of microparticles around a much larger agglomerate (10–20  $\mu\text{m}$ ), explained by ion flux from the homogeneous ambient plasma of inductively coupled rf discharge to the surface of the agglomerate, was first experimentally observed and published in Ref. [24]. The motion of a droplet consisting of microparticles inside a dust-free region of a capacitive coupled rf discharge was reported in Refs. [25,26]. The stability of the droplet can be explained, similarly to the capture of small microparticles around a large agglomerate, by the compression of the microparticle suspension due to plasma fluxes [26]. This effect is alike to compacting of cold molecular clouds with bright rims by surrounding highly ionized hot plasma according to radiation driven implosion model [27–29]. The implosion model attributes the compression of a cold molecular cloud by the ejection of plasma from a bright rim irradiated by newly formed stars, and is in fact a rocket effect [30]. Thus, this is the main difference from microparticle cloud compression in gas-discharge plasma, where the plasma flux into the cloud is the result of plasma recombination on the surface of the microparticles of the cloud itself.

New experiments were performed on the PK-4 facility onboard the ISS under microgravity conditions [9] to study the fragmentation of a cloud of monodisperse microparticles followed by the collapse of fragments into dense globules by ion flux and the subsequent decay of the newly formed globules by a decrease of the ambient plasma density.

## II. CONDITIONS FOR DOMINATION OF MIROPARTICLES MUTUAL ATTRACTION

Usually, in laboratory complex plasmas the microparticles are confined in a self-consistent electrostatic trap formed in the plasma due to ambipolar diffusion to the chamber walls and microparticle surface. The main forces acting on a microparticle suspended in plasma in our experiment are as follows: electrostatic, ion drag, electron drag, neutral drag and thermophoretic [3,19]. We do not consider the thermophoretic force since the temperature gradients in our system are very low, at least on the scale of the interparticle distance. Typically, the electric forces on a microparticle in a stationary dust

structure dominate over the ion drag force, so the ambipolar diffusion field induced by the plasma flow out of the dust structure balances the repulsion of negatively charged grains from each other and keeps them trapped [31]. The plasma flow creates a drag force due to the momentum transfer to a charged grain by both, direct absorption of ions and electrons and deflection of their trajectories in the electric field of the grain. Thus, the ions, partially transferring momentum to the microparticle, play the role of Le Sage's corpuscles. The attraction between microparticles can appear if the plasma density and the microparticle number density increase so that the ion drag force due to the plasma flux onto the grains prevails over the repulsion by the electric force (the electron drag force is typically a order of magnitude lower than the ion drag force under the discharge plasma conditions [32] and is not considered).

The ion drag force can be calculated under binary collision approach [33] as

$$\mathbf{F}_i = m_i \int \mathbf{v} v \sigma(v) f(\mathbf{v}) d\mathbf{v}, \quad (1)$$

where  $m_i$  is the mass of ion,  $f(\mathbf{v})$  is the ion velocity distribution function, and  $\sigma(v)$  is the moment transfer cross section of ion-microparticle collision. For subthermal ion flow the velocity distribution function can be written as  $f(\mathbf{v}) \approx (1 + \mathbf{u} \cdot \mathbf{v} m_i / k_B T) f_0(v)$ , where  $\mathbf{u}$  is the ion flow velocity, and  $f_0(v)$  is the Maxwellian velocity distribution function. After integration (1) over angles and using energy  $\varepsilon = m_i v^2 / 2$  instead  $v$ , we obtain:

$$\mathbf{F}_i = \frac{4\mathbf{u}}{3m_i k_B T} \int \varepsilon^2 \sigma(\varepsilon) f_0(\varepsilon) d\varepsilon = \mathbf{J} \sqrt{m_i k_B T} \lambda_D^2 \xi, \quad (2)$$

where  $T$  is the gas temperature,  $\mathbf{J} = \mathbf{u} n_i$  is the ion flow,  $n_i$  is ion number density,  $\lambda_D$  is the Debye length, and  $\xi$  is the dimensionless parameter:

$$\xi = \frac{4\sqrt{2}}{3\sqrt{\pi} (k_B T)^3 \lambda_D^2} \int_0^\infty \sigma(\varepsilon) \varepsilon^2 \exp(-\varepsilon / k_B T) d\varepsilon, \quad (3)$$

The moment transfer cross section can be calculated according to Ref. [34] as

$$\sigma(\varepsilon) = 2\pi \int_0^\infty (1 - \cos \chi(b, \varepsilon)) b db, \quad (4)$$

where

$$\chi(b, \varepsilon) = \pi - 2b \int_{r_{\min}}^\infty \frac{dr}{r^2 \sqrt{1 - \frac{e\varphi(r)}{\varepsilon} - \frac{b^2}{r^2}}}, \quad (5)$$

$\varphi(r)$  is the potential distribution around the microparticle,  $e$  is the elementary charge, and  $r_{\min}$  is the turning point defined as the outmost zero of the function  $1 - \frac{e\varphi(r)}{\varepsilon} - \frac{b^2}{r^2}$  [34].

The potential distribution can be approximated by Yukawa potential  $\varphi(r) = (Q/4\pi \varepsilon_0 r) \exp(-r/\lambda_s)$ , where  $\lambda_s$  is the effective screening length [11]. The effective screening length is defined as  $\lambda_D \sqrt{1 + 0.48\sqrt{\beta}}$  [35], where  $\beta = -Qe/4\pi \varepsilon_0 \lambda_D k_B T$  is the Coulomb parameter. Under such assumptions the coefficient  $\xi$  depends only on the Coulomb parameter.

To calculate the microparticle charge and plasma flux onto its surface, a balance of the ion and electron fluxes can be used (see Appendix A). The plasma flux onto the microparticle  $I_p = I_i = I_e$  gives the plasma flow density decreasing with the distance  $r$  from the microparticle as

$$J_p = \frac{I_p}{4\pi r^2}. \quad (6)$$

If there is another microparticle around, then the plasma flow acts on it in a manner similar to the way corpuscles act on massive bodies in Le Sage's theory, and the force acting on this microparticle can be estimated by substituting Eq. (6) into Eq. (2):

$$F_p = \frac{I_p \sqrt{m_i k_B T} \lambda_D^2 \xi}{4\pi r^2}. \quad (7)$$

This, second, microparticle in turn also acts on the first one, thus the microparticles attract each other. These forces are basically nonreciprocal. Usually, wake formation in the presence of a relatively strong electric field is responsible for the nonreciprocity [36,37]. In the considered case, the electric field is weak enough to make the wake negligible, and the reason for the nonreciprocity can be the dependence of the force  $F_p$  on the microparticle size via  $I_p$  [see Eqs. (A1) and (A2)]. When the microparticles are identical, the forces become completely symmetric. Note that the attractive force (7) dependence on the distance is the same as for the gravitational force. The plasma flow  $J_p$  (6) also gives rise to an ambipolar diffusion electric field, which leads to a power dependence of the potential at a large distance from the microparticle [22]. When electrons are much hotter than ions this field can be estimated as  $E = J_p/n_i \mu_i$  at a distance larger than the ion mean free path, where  $\mu_i = e/m_i v_{\text{col}}$  is the ion mobility, and  $v_{\text{col}}$  is ion-neutral collision frequency. The attraction between the microparticles is dominated when the ion drag force  $F_p$  prevails over the electric force  $EQ$  [38] or, using Eqs. (6)–(7),  $(m_i k_B T)^{1/2} \lambda_D^2 \xi > Q/n_i \mu_i$ . Assuming that the Debye length is close to the Debye length of ions, the last relation can be rewritten as

$$\lambda_D < \frac{\sqrt{m_i k_B T} \xi \mu_i}{4\pi e \beta} = \frac{\xi l_i}{4\pi \beta}, \quad (8)$$

where  $l_i = (k_B T/m_i)^{1/2}/v_{\text{col}}$  is the ion mean free path length. This condition is similar to the one derived in Ref. [38]. So, the attraction between microparticles can arise only in a dense enough plasma.

At the same time, the condition (8) implies that the confining force of the ambipolar electric field becomes weaker than the ion drag force caused by plasma diffusion to the chamber walls, and therefore the particles are pushed away from the central region of the discharge. Thus, the attraction between microparticles occurs only as long as they remain in the central region of the discharge, where the plasma density is high. Hence, the observation of the fragmentation of the microparticles cloud, followed by contraction of the fragments, is only possible before the microparticles have been pushed out to the periphery. In addition, to maintain the ion flux responsible for the mutual attraction of a group of microparticles, the plasma recombination on the microparticles of this group should exceed the ionization in the region occupied by

this group. The latter condition can be written as

$$n_p > v_i n_e / I_p, \quad (9)$$

where  $v_i$  is the ionization rate,  $n_p$  and  $n_e$  are the number densities of microparticles and electrons respectively.

Typically, laboratory experiments with complex plasmas do not fulfill the conditions (8) and (9). We therefore developed a new experimental technique to increase both the plasma density and microparticles number density, which allowed us the direct observation of the mutual attraction of microparticles in the ISS based PK-4 facility.

### III. EXPERIMENTAL SETUP

The heart of the PK-4 installation is the plasma chamber, which constitutes a glass discharge tube with 3-cm inner diameter and a length of 85 cm. The electrodes are attached at the two ends of the chamber and create a dc discharge between them. Two rf coils (one movable along the tube axis and one fixed) are able to generate an rf plasma in addition to the dc discharge. In our experiment the coils were located in the middle of the plasma chamber far from the dc electrodes and 5.5 cm apart from each other. The neon gas pressure in the plasma chamber is maintained by a gas flow and pressure control system. The roles of anode and cathode can be interchanged, allowing to reverse the polarity of the dc discharge field. A set of lenses shapes the illuminating laser beam illuminate a thin slab of microparticles. The slab minimum thickness is about 100  $\mu\text{m}$  at the 10% intensity level and grows parabolically across the cameras field of view up to 440  $\mu\text{m}$ . Two high resolution cameras acquire images of illuminated microparticles in a  $44 \times 3.8 \text{ mm}^2$  field of view at a frame rate of up to 100 fps. The camera image scaling is around 14.25  $\mu\text{m}/\text{pixel}$ . The third camera captures image of the plasma glow in three spectral intervals: around 585 nm, around 703 nm and in the entire visible range. For further details, please refer to Ref. [9].

### IV. EXPERIMENTAL PROCEDURE

The experiment stages are illustrated schematically in Fig. 1. Overall, five stages of the experiment can be highlighted, i.e., a preparation stage, two data gathering stages and one recovery stage. In a first “*collection*” stage a suspension of 3.38- $\mu\text{m}$ -diameter monodisperse microparticles was initially trapped in a combination of low-power rf (0.4 W) and dc (0.5 or 1 mA) discharges maintained concurrently in neon at a pressure of 30 Pa (we will call this combination as a combined discharge further on). RF power was applied to the movable coil only. We counted the number of microparticles in a square image region of  $200 \times 200$  pixels at the end of this stage. A typical microparticle number density was  $n_p \approx (9 \pm 2) \times 10^4 \text{ cm}^{-3}$ . Thus, the relation (9) was far from fulfillment. To achieve the high microparticle density required in (9), we go to second, a “*wave development*” stage. During this stage we completely shut off the rf discharge and changed the polarity of the dc discharge to make the microparticles drift in the direction from the moving coil to the stationary one as shown in Fig. 1(a). Then, when the microparticles suspension gained

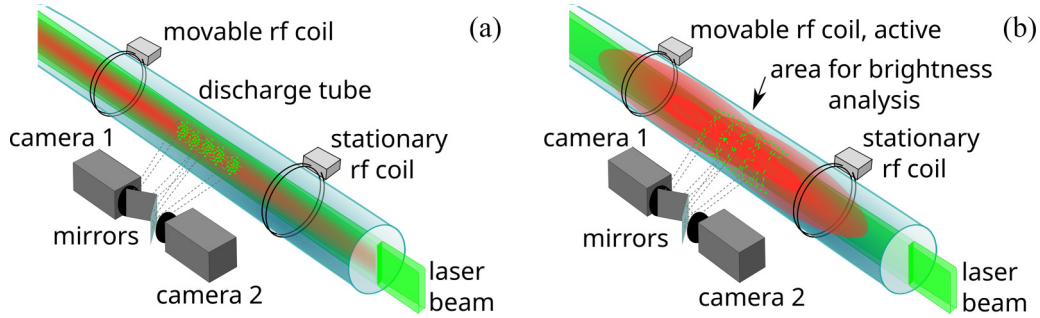


FIG. 1. Schematic of the two main stages of the experiment: (a) microparticle suspension (green circles) drifting in a pure dc discharge (red) in neon, dust-acoustic waves excited due to the ion drift; (b) high rf power discharge (red) activated by movable rf coil, microparticles moving away from the discharge axis, meanwhile, part of them collapsing into dense globules. A thin slab of microparticles is illuminated by the accordingly shaped laser beam. Two high-resolution cameras collect the light scattered by microparticles.

speed, dust-acoustic self-excited waves developed similarly to Refs. [39,40] showing a much higher microparticles number density  $n_p = (3-7) \times 10^5 \text{ cm}^{-3}$  in the wave crests. Waves were nonlinear with sharp wave crests of width within 0.2–0.5 mm. It is not possible to resolve individual microparticles in a wave crest. Therefore, we use the brightness averaged over a region of  $6 \times 6$  pixels in the waves crests to determine the microparticle number density and the fact that particle observation cameras are linear. As a calibration point, we take the microparticle number density obtained at the end of the previous stage and the brightness averaged over the same region where we have counted the microparticles. The overall error in determining the microparticle number density is about 30%.

Although we were able to satisfy (9) in the wave crests, the plasma density  $n_e^{\text{dc}} = 2.0 \times 10^8 \text{ cm}^{-3}$  [9] is yet too low to satisfy (8). To increase the plasma density we proceed to the “main,” third stage and abruptly feed high, 2–5 W, power to the movable rf coil to increase the number of electrons to meet the condition of (8). In spite of feeding only the movable rf coil, the plasma glow filled the entire space between the two coils due to their mutual coupling [Fig. 1(b)] in this stage. We estimate the temperature and concentration of electrons in this stage of our experiment as  $\sim 4 \text{ eV}$  and  $\sim (3-8) \times 10^9 \text{ cm}^{-3}$ , depending on the rf power (see Appendix B). Calculation of the microparticle charge and the Coulomb parameter based on the estimated plasma parameters is presented in Appendix A. The microparticle charge  $Z_p$  and the Coulomb parameter  $\beta$  are shown in Fig. 8 (Appendix A). They lay in the range 3600–4900  $e$  and 10–22, respectively. Besides, based on the Appendix A, the typical plasma flux on a microparticle is  $\sim (0.7-1.4) \times 10^{10} \text{ s}^{-1}$ . Note, the timescale of microparticle charging is less than 1  $\mu\text{s}$ , which allows us to consider the charge of the microparticles to be in equilibrium with the surrounding plasma for analysis of the microparticle dynamics.

We have allowed the microparticle cloud to evolve for 0.1–0.5 s at this *main* stage with high rf power, and then restore the rf power to the initial, “trapping” value, thus, entering the forth, “relaxation” stage. Finally, we met a fifth, a “recollection” stage and restored the dc current polarity too to pull the microparticles suspension back, to its original position, for a reiteration of the experiment sequence to the *main* stage.

## V. EXPERIMENTAL RESULTS

### A. Microparticles mutual attraction

A visual demonstration of the 3.38- $\mu\text{m}$  microparticle motion during the experiment is shown by the image sequence acquired at 70 fps in Fig. 2. The microparticles are actually displayed as elongated tracks due to their rapid motion and the long, 14 ms exposure time. The neon pressure was 40 Pa in this example for better pronounced microparticle trajectories, although most other experiments were conducted at 30 Pa. We assigned the time  $t = 0 \text{ ms}$  to the frame when the 3-W rf power was fed. Thus, the frame before the burst of rf power

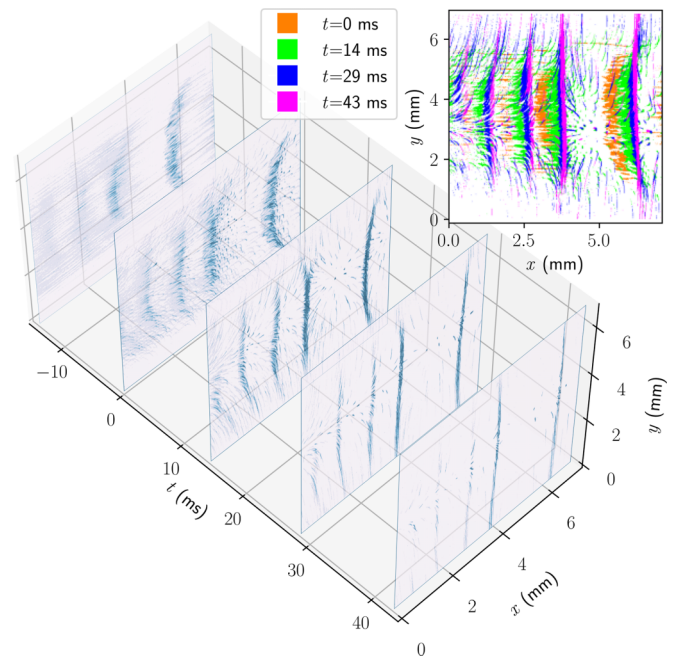


FIG. 2. Subsequent images from camera 1 demonstrate experiment sequence at 40-Pa neon pressure and exposure time 14 ms.  $t = 0 \text{ ms}$  is assigned to the frame when 3-W rf power was switched on. The waves stop propagating at  $t > 0 \text{ ms}$ . The frames at  $t = 14 \text{ ms}$  and  $t = 29 \text{ ms}$  reveals compaction and thickening of the wave crests. Some particles exhibit retromotion being pulled into the crests. Inset is a colored overlay of the same consequent frames.

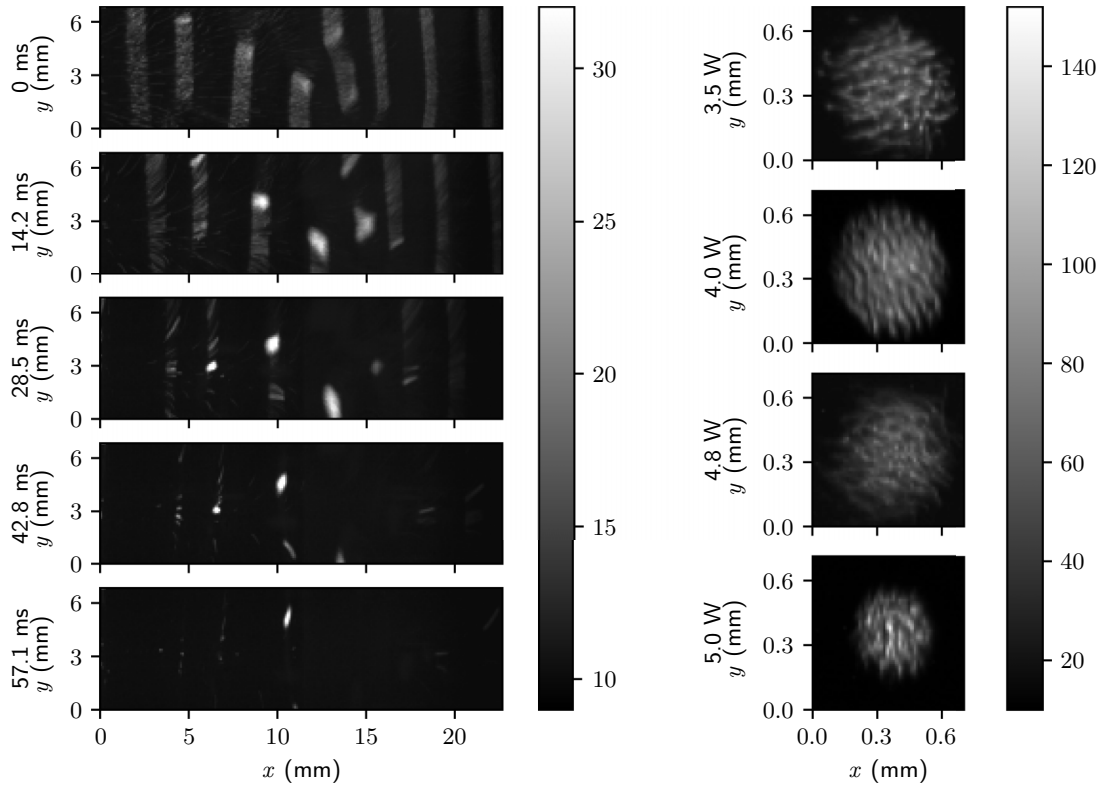


FIG. 3. Left panel: Evolution of a  $3.38\text{-}\mu\text{m}$  microparticle suspension after 5-W rf power feed; showing consecutive frames at 70 fps (top to bottom). First frame shows eight already slightly deformed dust acoustic wave crests. The brighter blobs reflect the beginning of the fragmentation process and globule formation. The second frame, 14.2 ms later, reveals deeper fragmentation, the globules pulled in more particles and looks brighter. The third frame reveals only the remnants of wave crests and developed globules. The globule in the middle at the bottom looks elongated, implying that this globule is slipping downward. The fourth frame shows well-developed globules. One only globule is visible in the fifth frame, escaping the field of view upward. Right panel: examples of  $3.38\text{-}\mu\text{m}$  microparticle globules at different rf powers. The internal structure of the globules is visible, although the particles are streaked due to the globule motion. The gray bars show the conversion of the raw image sensor readings to the presented images.

shows dust acoustic waves in a suspension of microparticles, drifting in a pure dc discharge. As soon as the rf discharge developed, the axial dc field in plasma decreased because the dc current remains, while the conductivity increases by an order of magnitude and, thus, the waves almost stopped propagating. At the same time the wave crests became much more compact and narrow in the axial direction caused by the attraction of microparticles, and later began to thin due to the expansion of the cloud in the radial direction, dragged by the plasma flow to the wall of the tube. The superposition of a sequence of colored frames in the inset of Fig. 2 shows the same process. The inset, on par with the main view, reveals that the wave crests have stopped propagating to the right at  $t > 0$  ms, but the microparticles exhibit retromotion in some areas, e.g., at  $x$  in the range 4.0–5.0 mm and 6.2–7.0 mm, indicating the ion drag force toward the crest of the wave. Similar crest compaction followed by radial expansion also occurs at higher rf power.

### B. Globule formation

During the *main* stage of the experiment along with the compacting of wave crests, we also observed fragmentation in the plane of the wave crest in a number of experimental runs,

and furthermore, sometimes these fragments collapsed into dense globules. An example of fragmentation and globules formation in the wave crest plane is shown in the left panel of Fig. 3. The upper frame shows the moment when the 5-W rf power was applied. Eight already slightly deformed dust acoustic wave crests like those shown in Fig. 2 are visible. Some of the wave crests show brighter blobs. These blobs reflect the fragmentation process and the beginning of globule formation. The second frame, 14.2 ms later, shows further fragmentation progression—the wave crests look ripped, the much brighter blobs evidence more neighboring microparticles pulled into the globules. The third frame reveals only the remnants of wave crests and a few even brighter blob-globules. Some of the developing globules escaped from the field of view either vertically (according to the image) or out of the laser illuminated plane. Note: The globule in the middle at the bottom looks elongated, implying that this globule is speeding up to slip downward. In the fourth and fifth frames one can see already well-developed globules, although the globule in the fifth frame looks smeared, as it has already gained speed in the radial direction.

From the left panel of Fig. 3, it is evident that the position in which the globules are formed is quite random. So, only a small fraction of the globules illuminated by the laser can

be observed. Globules, as well as individual microparticles, had a tendency to be repelled from dense plasma region due to plasma diffusion flux, but dense globules drifted from the tube axis considerably slower than individual microparticles. This effect can be explained by a decrease in the ion drag force in the dense suspension due to screening of the ion flux by the surrounding microparticles [41]. Despite this, the observation time never exceeded 0.15 s because the globules escaped either the laser sheet or the field of view very soon.

We investigated the globule production at 2.0–5.0 W rf power fed to the moving rf coil and found that 2.0 W power led only to a radial expansion of the microparticle suspension. The first evidence of microparticle mutual attraction occurred at 3.0 W, but no compact globules were observed. Only at powers above 3.5 W the microparticle suspension spreads into compact globules. The globules slowly crossing the illuminating laser waist are of most interest for further analysis, see, e.g., the right panel of Fig. 3.

The spatial distribution of microparticles at the start of fragmentation, i.e., at the moment of rf power feed, is the distribution of microparticles in the crest of a nonlinear dust-acoustic wave. It depends on the steady-state number density of microparticles just before the start of the suspension drift in the pure dc discharge and on the delay from the drift onset to the moment of the rf power feed, but it does not depend on the rf power value itself.

The majority of the observed globules had an almost spherical shape with a diameter of 0.15–1.1 mm and a number of microparticles from a few tens to thousands. For the globules in which individual microparticles could not be recognized, we made an estimation of the microparticle number density in globules in the same manner as we did in Sec. IV for the microparticles number density in the wave crests (Fig. 4).

### C. Globules disintegration

We have also observed the disintegration of globules in a number of our experiments during the *relaxation* stage (Sec. IV). To observe the globule disintegration, the plasma density has been sharply decreased by reducing the rf power at the end of the *main* stage (Sec. IV), when the globule is in the observation area yet. Figure 5 shows the time and spatial resolved evolution of a suspension of microparticles into a single globule at 4-W rf power during 0.1 s and then its disintegration. In this case,  $t = 0$  s corresponds to the moment when the high rf power reverted back to a low value, so that the attraction by the ion drag force, driven by the plasma flux from the surrounding high-density plasma, was drastically reduced. This very moment is shown in green and looks like a starfish with protruding beams—the individual microparticles started to shoot out of the globule. The process of the globules disintegration due to the ambient plasma rarefaction at the moment of rf power drop is yet another proof that the mechanism of microparticles mutual attraction by the plasma flux actually is in effect. Notice that the globule moves at an acute angle to the plane of the laser beam, so it has already partially left the illuminated region when the decay begins. Actually, this allows a better observation of individual microparticles shooting out of the globule under the action of the screened Coulomb force, no longer compensated by the attraction. The

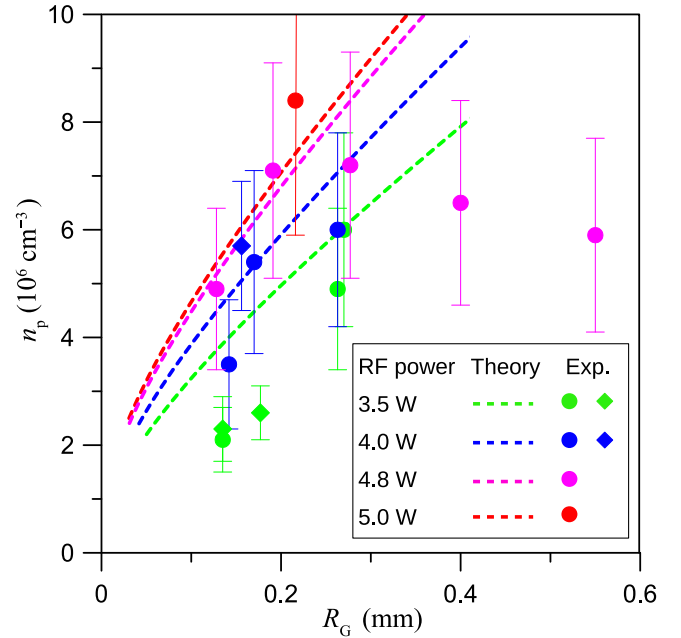


FIG. 4. Density of 3.38- $\mu\text{m}$  microparticles globules versus its radius for rf power of 3.5 W in green, 4 W in blue, 4.8 W in magenta, and 5 W in red; circles represent densities determined by brightness method, diamonds by counting microparticles; solid lines theoretical estimation in accordance with Eq. (13). The error bars indicate the overall error in determination of the microparticle number density.

images of the shooting out microparticles after the rf power reduction are shown consecutively in green, dark blue, brown, and magenta in Fig. 5.

The observation of a globule disintegration also allows an independent estimate of the number density inside the globule. After the globule “explosion” the shot out microparticles crossed the laser sheet during four frames and were counted as 45 individual microparticles. Taking into account that the globule begins to disintegrate right after crossing the laser beam, and assuming the symmetry of the “explosion”, about half of the microparticles only pass through the laser beam and are counted. Thus, we can estimate the total number of microparticle in the globule as 90. The size of this globule was  $0.31 \pm 0.014$  mm and hence the mean globule density approximately equal to  $(5.7 \pm 1.7) \times 10^6 \text{ cm}^{-3}$ . The diamonds in Fig. 4 show the number density obtained by counting the microparticles. The number density obtained from the globule disintegration shows a good agreement with the density estimated by the brightness method (circles in Fig. 4).

## VI. DISCUSSION

### A. Analog to gravitational instability

Although the relations (8) and (9) show the conditions of mutual attraction of microparticles, they are not sufficient for the observed fragmentation and collapse of microparticles into globules since they do not account for short-range repulsion. Since the mutual attraction of microparticles is described by Le Sage-like gravitation, alike that of massive bodies, let us try to apply the concept of gravitational instability as a guide

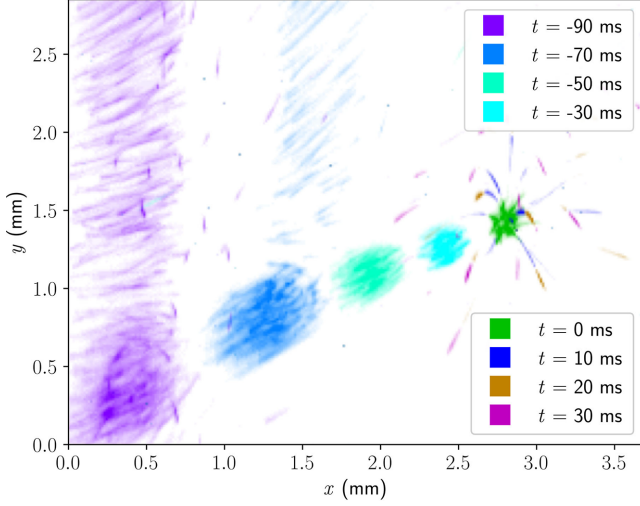


FIG. 5. Temporal and spatial resolved evolution of a suspension of microparticles into a single globule followed by disintegration. The colors represent unevenly temporally distributed images with an exposure time of 10 ms. The globule moves at an acute angle to the plane of the laser beam, so it has already partially left the illuminated region by the beginning of decay. The image of  $t = 0$  s shows the beginning of the globule disintegration in green. The following dark blue, brown, and magenta tracks, show the individual microparticles shooting out of the globule at the later time intervals.

to understand the onset of fragmentation and/or collapse of microparticle clouds.

The Jeans length [42] gives a useful criterion for the onset of gravitational instability [43,44]:

$$L_J = \sqrt{\frac{\pi}{Gm^2n} \frac{\partial P}{\partial n}}, \quad (10)$$

where  $m$  and  $n$  are the mass of primitive elements and number density of the massive cloud,  $P$  is the pressure in the cloud and  $G$  is the gravitational constant. Roughly, if the cloud is larger than Jeans length, then it can collapse. This criterion only provides a basic insight into the collapse of self-gravitating systems under the assumption that it is formulated in the small perturbation approach. Moreover, it does not take into account the angular momentum of the system and many other phenomena, such as turbulence, radiative processes, internal energy sources, etc. [45–51]. In contrast, the microparticles of our complex plasma system are immersed in an albeit rarefied but fairly dense neutral gas, therefore spin, turbulence and heating are effectively inhibited.

The equivalent of the Jeans length for a microparticle suspension is

$$L = 2\pi \sqrt{\frac{1}{I_p \sqrt{m_i k_B T} \xi \lambda_D^2 n_p} \frac{\partial P}{\partial n_p}}, \quad (11)$$

which is derived from Eq. (10) by substitution  $I_p \sqrt{m_i k_B T} \xi \lambda_D^2 / 4\pi$  from Eq. (7) instead of  $Gm_p^2$ , taking into account the same dependence of the gravitational force on the distance. Notice we have chosen a form of Eq. (10) that does not involve any particular equation of state which can be substituted into  $\partial P / \partial n_p$ . The pressure of the microparticle

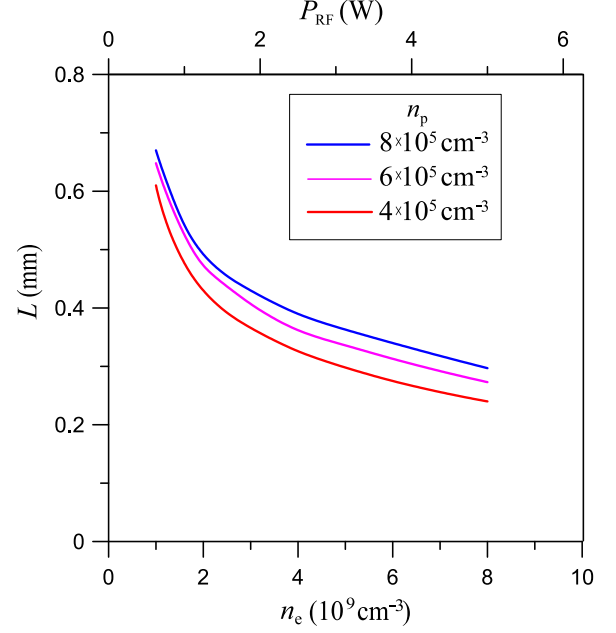


FIG. 6. Dependence of the Jeans length equivalent  $L$  in complex plasma on electron number density for the 3.38- $\mu\text{m}$  microparticles number densities  $n_p = 4, 6,$  and  $8 \times 10^5 \text{cm}^{-3}$ .

subsystem of the complex plasma should be used in Eq. (11). The latter is determined mainly by short-range interactions among microparticles, constituting a strongly coupled system. Debye-Hückel (Yukawa) model is widely used to describe such systems [3,10]. A practical expression of the pressure of those systems can be found in Ref. [52] (see Appendix C). The Jeans lengths for the ion drag attraction instability calculated according Eq. (11) are shown in Fig. 6.

In our system the gravitational-like instability emerges amid initial stochastic fluctuations of the number density of microparticles in the wave crests. The scale of these fluctuations is of the order of the wave crest width. On the other hand, for collapse to be even remotely probable, the size of the fluctuation must be larger than the Jeans-like length [Eq. (11)]. The Jeans length presented in Fig. 6 is close to the widths of the wave crests, hence the formation of globules is quite possible. Notice that the Jeans length decreases as the rf power increases, which increases the probability of collapse into globules, in agreement with our observations.

### B. Microparticles number density in globules

Along with the experimental estimation of the microparticle number density in globules, an analytical one has been performed. Assuming that the momentum of the total ion flux onto the microparticles inside the globule is applied to the surface of the globule itself, we can make an upper estimate of the pressure exerted by this flux on the globule surface:

$$P = \frac{N_p}{4\pi R_G^2} I_p \sqrt{m_i k_B T} / 2, \quad (12)$$

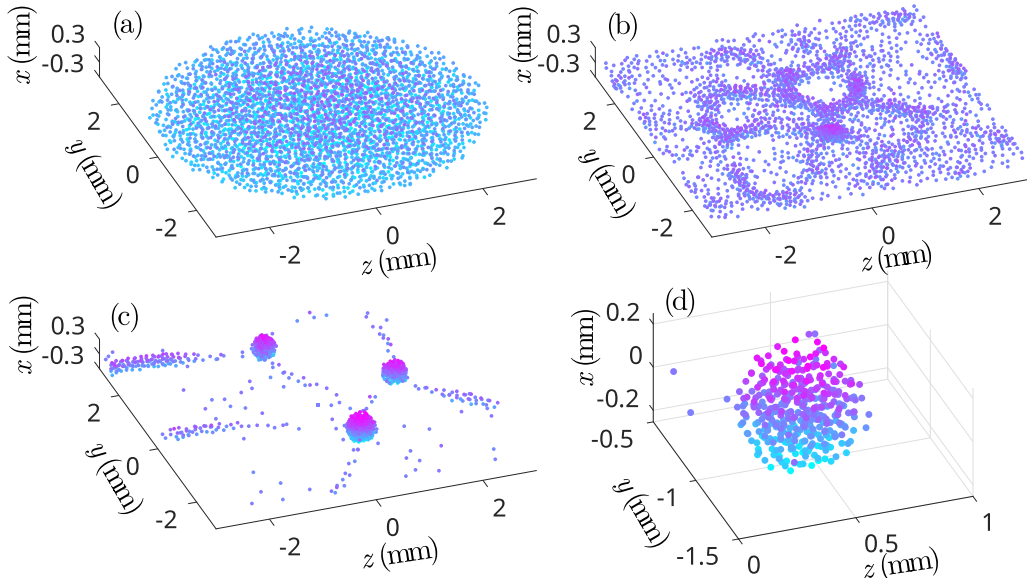


FIG. 7. Molecular dynamic simulation of evolution of the microparticle suspension in the single wave crest. (a) The initial state,  $t = 0$  ms; (b) the fragmentation development  $t = 30$  ms later; (c) the collapse into the globules after  $t = 60$  ms evolution; (d) one of the well-developed globules (magnified). Particles are colored along  $x$  axis.

where  $N_p$  is the total number of microparticles in the globule,  $R_G$  is the globule radius, and  $I_p$  is the ion flux on a microparticle. Substituting  $N_p = \frac{4\pi}{3}R_G^3 n_p$ , Eq. (12) can be written as

$$P = \frac{n_p}{3} R_G I_p \sqrt{m_i k_B T} / 2. \quad (13)$$

The pressure (13) should be balanced by the globule internal pressure from Eq. (C1). The resulting algebraic equation was solved numerically. The results are shown in Fig. 4. Both experimental and theoretical densities inside the globule exhibit similar dependencies on the ambient plasma density (rf power). The above densities also have similar dependencies on globule radii up to 0.3 mm. The high discrepancy in Fig. 4 for globule radii above 0.3 mm is explained by the deviation of the plasma density inside the globule from the ambient one, when the globule size substantially exceeds the ion mean free path (about 0.17 mm for our plasma). For a larger globule the average equilibrium microparticle number density should be lower than the result given by the Eq. (13).

## VII. MOLECULAR DYNAMICS SIMULATION

The microparticle suspension fragmentation and following contraction into globules were also simulated using the molecular dynamics (MD) technique [53]. The physical conditions were about the same as in the experiments at 4.0-W rf discharge power (see Appendix D for the simulation details). Figure 7(a) shows the initial distribution of the microparticles in the model of the experimental single wave crest. The first 30 ms of the MD simulation show the radial expansion, thinning along the axis and fragmentation of the initial microparticle cloud [Fig. 7(b)]. The radial expansion and the thinning are very similar to the experimental observations, e.g., shown in Fig. 2. The fragmentation is identical to the one illustrated in

the left panel of Fig. 3. The contraction of the fragments into dense globules after 60 ms evolution can be seen in Fig. 7(c). Thus, comparing this figure with Fig. 3 and 5, we can conclude that the timescales of globule contraction are very much alike to the experiments. Finally, Fig. 7(d) demonstrates one well-developed globule with a resolved interior structure. The density of the simulated globules is significantly higher than that observed in the experiments (Fig. 4) and estimated from Eq. (13). This difference can be explained as the expressions (7) and (D3) for the interaction force of a pair of microparticles, used for the MD simulation, are only accurate when the interaction of the microparticles with the ion flux is not perturbed by other neighboring microparticles. But in a dense globule, this assumption is no longer correct, because the length scale defined by the effective cross section of the momentum transfer from the ion stream to the microparticle now exceeds the interparticle distance. So the ion stream, which gave momentum to a single particle, is now sharing it with many. This effect is taken into account in Eq. (13) because the combined cross section of the interaction of the ion flux with the microparticles in the globule is substituted by the area of the globule surface in this equation.

## VIII. CONCLUSION

We observed the formation of globules of microparticles in complex plasmas performing experiments with the PK-4 facility onboard the ISS. The microparticles injected into the dc neon plasma drifted in the longitudinal electric field of the discharge and showed at low pressures self-excited waves caused by a two-stream instability of the microparticles drifting against the ions. When we powered one of the external rf coils the microparticles in the crest of the waves, where the microparticle density is the highest, started to form globules of microparticles consisting of 10 to 1000 microparticles.



As soon as the rf discharge was switched off, the globules disintegrated quickly.

The formation of globules in this experiment is explained by the radial ion flux to the microparticles in the high density regions of the waves leading to a mutual attraction between the microparticles. The collapse of the microparticle clouds is similar to the formation of stars in interstellar molecular clouds, including the cloud fragmentation prior to the collapse. Instead of the gravitational force, however, the attraction between the particles is produced by the radial flux of the ions. In this sense, the attraction is caused by the Le Sage mechanism, which was used to explain the gravitational attraction by corpuscles streaming isotropically through the Universe. The use of the expression for the Jeans length, which provides guidance on the conditions for the onset of gravitational instability of interstellar clouds, with the replacement of the gravitational contribution by the ion flux yield a spatial scale of perturbation for globule formation onset close to the width of wave crests. In addition, we performed MD simulations leading to similar results.

In this work, we have shown that complex plasma experiments can be used to simulate the gravitational collapse, purified from some of perturbations inherent to interstellar processes, and the Le Sage mechanism for explaining the gravity-like attraction. This is one more proof that complex plasmas are useful as a model to understand the behavior of many-body systems.

#### ACKNOWLEDGMENTS

All authors greatly acknowledge the joint ESA-Roscosmos “Experiment Plasmakristall-4” onboard the International Space Station. This work was supported by the Ministry of Science and Higher Education of the Russian Federation (State Assignment No. 075-00270-24-00). M.H.T. was supported by DLR under Grant No. 50WM2044. We thank M. Y. Pustynnik and H. M. Thomas for the joint productive experiments in 2021. We also very thankful to S. A. Khrapak and A. V. Ivlev for helpful discussions and comments.

#### APPENDIX A: MICROPARTICLE CHARGE AND PLASMA FLUX DETERMINATION

The electron flux is

$$I_e = n_e r_p^2 \sqrt{\frac{8\pi k_B T_e}{m_e}} \exp\left(\frac{e\varphi_s}{k_B T_e}\right) (1 - R_e), \quad (\text{A1})$$

where  $n_e$  is the electron number density;  $r_p$  and  $\varphi_s$  are the microparticle radius and floating potential, respectively;  $R_e = 0.6$  is the reflection coefficient of electrons from the grain surface [54]. The ion flux can be expressed as [55]

$$I_i = I_{\text{OML}} + I_{\text{col}} = r_p^2 n_i \sqrt{\frac{8\pi k_B T}{m_i}} \left(1 - \frac{e\varphi_s}{k_B T}\right) + \frac{4\pi}{3} R_0^3 n_i \nu_{\text{col}}, \quad (\text{A2})$$

where  $m_i$  is the mass of the ion,  $R_0 = \lambda_D \ln(1 + \beta)$  is the effective capture radius and  $\nu_{\text{col}}$  is the collision frequency of ions with neutrals. The balance of the electron and ion fluxes gives a value of the surface potential of the microparticle in

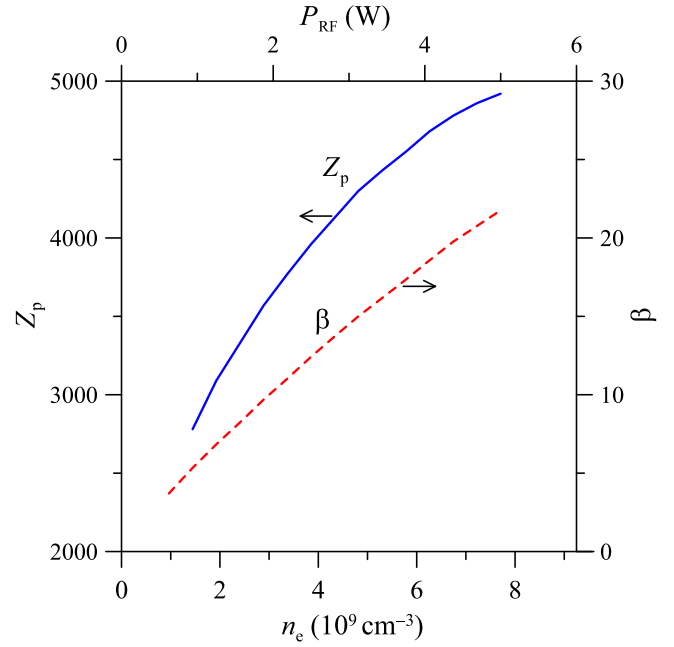


FIG. 8. The charge  $Z_p$  (in electron charges) and Coulomb parameter of  $3.38 \mu\text{m}$  microparticles in combination of inductively coupled rf at different powers and 1-mA dc discharges maintained concurrently in neon at 30-Pa pressure.

steady-state conditions. The charge can be determined from the surface potential using Coulomb’s law if the particle radius is smaller than the Debye length. The results of the microparticle charge calculation as well as the determined Coulomb parameter for the experimental plasma conditions estimated in Appendix B are presented in Fig. 8.

#### APPENDIX B: PLASMA PARAMETERS ESTIMATION

The level  $2p_1$  of neon is excited by a direct electron impact from the ground state and does not depend on metastable atoms concentration, thus the neon glow intensity at a 585-nm wavelength is proportional to the electron number density. We measured the intensity  $I_{\text{rf}}$  of the 585-nm line in the combined discharge at different rf power and intensity  $I_{\text{dc}}$  at 1-mA dc current in the area indicated by the arrow in Fig. 1(b). It turned out that the intensity dependence is almost linear. Assuming that the electron number density in dc discharge of 1-mA current is  $n_e^{\text{dc}} = 2.0 \times 10^8 \text{ cm}^{-3}$  [9], we can estimate the electron number density in the combined discharge with rf power of  $P_{\text{rf}}$  as

$$n_e = n_e^{\text{dc}} \left(\frac{I_{\text{rf}}}{I_{\text{dc}}}\right) = 1.6 \times 10^9 \text{ cm}^{-3} \left(\frac{P_{\text{rf}}}{\text{W}}\right). \quad (\text{B1})$$

The effective electron temperature in the combined discharge (which is similar to pure inductive rf discharge at the large rf powers) can be taken as 4 eV [56]. Assuming a Besselian radial distribution of electron number density, we can estimate the ionization rate:

$$\nu_i = D_a \mu_0^2 / R_i^2, \quad (\text{B2})$$

where  $D_a$  is ambipolar diffusion coefficient,  $\mu_0 \approx 2.405$  is first zero of the Bessel function, and  $R_i = 1.5 \text{ cm}$  is the

discharge tube radius. The equation (B1) allows the estimation of the microparticle charges and the Coulomb parameters for different discharge powers.

### APPENDIX C: PRESSURE IN STRONGLY COUPLED YUKAWA SYSTEM

The pressure of the Yukawa system can be estimated following [52]:

$$P = \frac{\kappa^4 \Gamma n_p k_B T_p}{6(k \cosh(\kappa) - \sinh(\kappa))^2} = \frac{3^{1/3} Q^2}{6(4\pi)^{4/3} \varepsilon_0 \lambda_s^4 (\kappa \cosh(\kappa) - \sinh(\kappa))^2}, \quad (\text{C1})$$

where  $\Gamma = (4\pi n_p/3)^{1/3} Q^2/4\pi \varepsilon_0 k_B T_p$  is the coupling parameter of the Yukawa system,  $T_p$  is the kinetic temperature of the microparticles, and  $\kappa = (4\pi n_p/3)^{-1/3}/\lambda_s$  is the screening parameter. The pressure derivative on the number density is

$$\frac{\partial P}{\partial n_p} = \frac{3^{1/3} Q^2 k^5 \sinh(\kappa)}{9(4\pi)^{4/3} \varepsilon_0 \lambda_s^4 (\kappa \cosh(\kappa) - \sinh(\kappa))^3} \approx \frac{\beta \lambda_D k_B T Z k^5 \sinh(\kappa)}{14.5 \lambda_s (\kappa \cosh(\kappa) - \sinh(\kappa))^3}, \quad (\text{C2})$$

where  $Z = -Q/e$  is the charge number of the microparticle.

### APPENDIX D: MOLECULAR DYNAMIC SIMULATION

Resting microparticles with an average number density of  $4 \times 10^5 \text{ cm}^{-3}$  were randomly placed in a ellipsoid of 6 mm diameter and 0.5 mm height prior to the simulation start. The shape of the cylinder is similar to a single wave crest. Initial distance between microparticles was larger than 50  $\mu\text{m}$ .

The interaction between microparticles is characterized by a superposition of Yukawa repulsion and gravity-like

attraction [Eq. (7)]:

$$U(r) = \frac{Q^2}{4\pi \varepsilon_0 r} \exp\left(-\frac{r}{\lambda_s}\right) - \frac{I_p \sqrt{m_i k_B T} \lambda_D^2 \xi}{4\pi r} \quad (\text{D1})$$

Let us take rf power  $P_{\text{rf}} = 4\text{W}$ . Then the electron and ion densities can be estimated as  $n_e = n_i = 6.4 \times 10^9 \text{ cm}^{-3}$ , in accordance with Appendix B. Debye length under this conditions is  $\lambda_D = 14.1 \mu\text{m}$ . Now we estimate a microparticle charge based on Appendix A  $Q = 4620e = -7.5 \times 10^{-16} \text{ C}$  ( $\beta = 18.4$ ) and the plasma flux on a microparticle  $I_i = 1.2 \times 10^{10} \text{ s}^{-1}$ . Effective screening length for given parameters in accordance with [35] is  $\lambda_s = \lambda_D \sqrt{1 + 0.48\sqrt{\beta}} = 24.6 \mu\text{m}$ . Numerical solution of Eqs. (3)–(5) yields  $\xi = 100.4$ . Thus,  $Q^2/4\pi \varepsilon_0 = 4.9 \times 10^{-21} \text{ J m}$  and  $I_p \sqrt{m_i k_B T} \lambda_D^2 \xi/4\pi = 2.24 \times 10^{-22} \text{ J m}$

Finally, the interaction potential is

$$U(r) = \frac{4.9 \times 10^{-21}}{r} \exp(-40600 \times r) - \frac{2.24 \times 10^{-22}}{r}, \quad (\text{D2})$$

which gives us the force exerted by the microparticle  $i$  on the microparticle  $j$ :

$$\mathbf{F}_{ij} = \frac{\mathbf{r}_{ji}}{r_{ji}^3} [4.9 \times 10^{-21} \exp(-40600 \times r_{ji}) \times (1 + 40600 \times r_{ji}) - 2.24 \times 10^{-22}], \quad (\text{D3})$$

(SI units), where  $\mathbf{r}_{ji}$  is the vector from the microparticle  $j$  to the microparticle  $i$ . The microparticle  $i$  is also subjected to the radial ion drag force toward the chamber wall:

$$F_\rho = J_\rho \sqrt{m_i k_B T} \lambda_D^2 \xi = 1.17 \times 10^{-10} \rho_i, \quad (\text{D4})$$

where  $\rho_i$  is the distance from the discharge axis to the microparticle  $i$ ;  $J_\rho = v_i n_e \rho/2$  and  $v_i = 1.56 \times 10^5 \text{ s}^{-1}$  is from Appendix B, Eq. (B2), assuming  $D_a \approx \mu_i (k_B T_e/e) = 6.06 \text{ m}^2 \text{ s}^{-1}$  [57]. The friction on the neutral gas was taken as  $85 \text{ s}^{-1}$  and a Langevin's thermostat of 300 K was applied. No other forces such as confinement or anything similar are imposed. The microparticles are free to leave the simulation cell. The mass of the microparticle was taken as  $3 \times 10^{-14} \text{ kg}$ , the time step in the simulation was 1  $\mu\text{s}$ .

- 
- [1] V. Fortov, A. Ivlev, S. Khrapak, A. Khrapak, and G. Morfill, Complex (dusty) plasmas: Current status, open issues, perspectives, *Phys. Rep.* **421**, 1 (2005).
- [2] G. E. Morfill and A. V. Ivlev, Complex plasmas: An interdisciplinary research field, *Rev. Mod. Phys.* **81**, 1353 (2009).
- [3] A. Ivlev, G. Morfill, H. Lowen, and C. P. Royall, *Complex Plasmas and Colloidal Dispersions: Particle-resolved Studies of Classical Liquids and Solids* (World Scientific, Singapore, 2012), Vol. 5, Chap. 2.2, p. 320.
- [4] J. H. Chu and L. I. Direct observation of coulomb crystals and liquids in strongly coupled rf dusty plasmas, *Phys. Rev. Lett.* **72**, 4009 (1994).
- [5] H. Thomas, G. E. Morfill, V. Demmel, J. Goree, B. Feuerbacher, and D. Möhlmann, Plasma crystal: Coulomb crystallization in a dusty plasma, *Phys. Rev. Lett.* **73**, 652 (1994).
- [6] Y. Hayashi and K. Tachibana, Observation of coulomb-crystal formation from carbon particles grown, *Jpn. J. Appl. Phys.* **33**, L804 (1994).
- [7] A. Melzer, T. Trottenberg, and A. Piel, Experimental determination of the charge on dust particles forming coulomb lattices, *Phys. Lett. A* **191**, 301 (1994).
- [8] M. H. Thoma, H. M. Thomas, C. A. Knapke, A. Melzer, and U. Konopka, Complex plasma research under microgravity conditions, *npj Micrograv.* **9**, 13 (2023).
- [9] M. Y. Pustyl'nik, M. A. Fink, V. Nosenko, T. Antonova, T. Hagl, H. M. Thomas, A. V. Zobnin, A. M. Lipaev, A. D. Usachev, V. I. Molotkov, O. F. Petrov, V. E. Fortov, C. Rau, C. Deysenroth, S. Albrecht, M. Kretschmer, M. H. Thoma, G. E. Morfill, R. Seurig, A. Stettner *et al.*, Plasmakristall-4: New complex (dusty) plasma laboratory on board the International Space Station, *Rev. Sci. Instrum.* **87**, 093505 (2016).

- [10] V. E. Fortov and G. E. Morfill, *Complex and Dusty Plasmas: From Laboratory to Space* (CRC Press, Boca Raton, FL, 2009), chap. 2.2, p. 418.
- [11] S. A. Khrapak and G. E. Morfill, Basic processes in complex (dusty) plasmas: Charging, interactions, and ion drag force, *Contrib. Plasma Phys.* **49**, 148 (2009).
- [12] A. M. Ignatov, Lesage gravity in dusty plasmas, *Plasma Phys. Rep.* **22**, 585 (1996).
- [13] Y. K. Khodataev, R. Bingham, V. P. Tarakanov, and V. N. Tsytovich, Mechanisms for the interaction of dust particles in plasmas, *Plasma Physics Reports* **22**, 932 (1996).
- [14] V. N. Tsytovich, Dust plasma crystals, drops, and clouds, *Phys. Usp.* **40**, 53 (1997).
- [15] Y. H. Chen and H. Luo, Static model for dusts in a plasma, *Phys. Plasmas* **6**, 699 (1999).
- [16] B. P. Resendes, J. T. Mendoca, and P. K. Shukla, Formation of dusty plasma molecules, *Phys. Lett. A* **239**, 181 (1998).
- [17] M. E. Marques and P. F. Williams, The electrostatic interaction of charged, dust-particle pairs in plasmas, *Phys. Lett. A* **278**, 152 (2000).
- [18] M. Lampe, G. Joyce, G. Gaunguli, and V. Gavrishchaka, Interactions between dust grains in a dusty plasma, *Phys. Plasmas* **7**, 3851 (2000).
- [19] S. A. Khrapak, A. V. Ivlev, and G. Morfill, Interaction potential of microparticles in a plasma: Role of collisions with plasma particles, *Phys. Rev. E* **64**, 046403 (2001).
- [20] S. A. Khrapak, G. E. Morfill, A. V. Ivlev, H. M. Thomas, D. A. Beysens, B. Zappoli, V. E. Fortov, A. M. Lipaev, and V. I. Molotkov, Critical point in complex plasmas, *Phys. Rev. Lett.* **96**, 015001 (2006).
- [21] S. A. Khrapak, G. E. Morfill, V. E. Fortov, L. G. D'yachkov, A. G. Khrapak, and O. F. Petrov, Attraction of positively charged particles in highly collisional plasmas, *Phys. Rev. Lett.* **99**, 055003 (2007).
- [22] S. A. Khrapak, B. A. Klumov, and G. E. Morfill, Electric potential around an absorbing body in plasmas: Effect of ion-neutral collisions, *Phys. Rev. Lett.* **100**, 225003 (2008).
- [23] R. Bingham and V. Tsytovich, New mechanism of dust growth and gravitation-like instabilities in astrophysical plasmas, *Astron. Astrophys.* **376**, L43 (2001).
- [24] A. D. Usachev, A. V. Zobnin, O. F. Petrov, V. E. Fortov, B. M. Annaratone, M. H. Thoma, H. Höfner, M. Kretschmer, M. Fink, and G. E. Morfill, Formation of a boundary-free dust cluster in a low-pressure gas-discharge plasma, *Phys. Rev. Lett.* **102**, 045001 (2009).
- [25] M. Schwabe, M. Rubin-Zuzic, S. Zhdanov, A. V. Ivlev, H. M. Thomas, and G. E. Morfill, Formation of bubbles, blobs, and surface cusps in complex plasmas, *Phys. Rev. Lett.* **102**, 255005 (2009).
- [26] E. Joshi, S. Khrapak, C. Knapek, P. Huber, D. Mohr, and M. Schwabe, Formation of droplets in weightless complex plasmas, *Contrib. Plasma Phys.* **61**, e202100081 (2021).
- [27] M. Sandford, R. W. Whitaker, and R. I. Klein, Radiation-driven implosions in molecular clouds, *Astrophys. J.* **260**, 183 (1982).
- [28] M. Sandford, R. W. Whitaker, and R. I. Klein, Radiatively driven dust-bounded implosions-formation and stability of dense globules, *Astrophys. J.* **282**, 178 (1984).
- [29] T. Kimura and M. Tosa, Shock propagation in a turbulent cloud, *Astrophys. J.* **406**, 512 (1993).
- [30] F. Bertoldi, The photoevaporation of interstellar clouds. i-radiation-driven implosion, *Astrophys. J.* **346**, 735 (1989).
- [31] M. Pustyl'nik, A. Pikalev, A. Zobnin, I. Semenov, H. M. Thomas, and O. Petrov, Physical aspects of dust-plasma interactions, *Contrib. Plasma Phys.* **61**, e202100126 (2021).
- [32] S. A. Khrapak and G. E. Morfill, Dusty plasmas in a constant electric field: Role of the electron drag force, *Phys. Rev. E* **69**, 066411 (2004).
- [33] S. A. Khrapak, A. V. Ivlev, G. E. Morfill, and H. M. Thomas, Ion drag force in complex plasmas, *Phys. Rev. E* **66**, 046414 (2002).
- [34] I. L. Semenov, S. A. Khrapak, and H. M. Thomas, Momentum transfer cross-section for ion scattering on dust particles, *Phys. Plasmas* **24**, 033710 (2017).
- [35] I. L. Semenov, S. A. Khrapak, and H. M. Thomas, Approximate expression for the electric potential around an absorbing particle in isotropic collisionless plasma, *Phys. Plasmas* **22**, 053704 (2015).
- [36] A. V. Ivlev, J. Bartnick, M. Heinen, C. R. Du, V. Nosenko, and H. Löwen, Statistical mechanics where newton's third law is broken, *Phys. Rev. X* **5**, 011035 (2015).
- [37] R. Kompaneets, Complex plasmas: Interaction potentials and non-hamiltonian dynamics, Ph.D. thesis, Ludwig-Maximilians-Universität München, 2007.
- [38] S. Khrapak and G. Morfill, A note on the binary interaction potential in complex (dusty) plasmas, *Phys. Plasmas* **15**, 084502 (2008).
- [39] S. Jaiswal, M. Pustyl'nik, S. Zhdanov, H. M. Thomas, A. Lipaev, A. Usachev, V. Molotkov, V. Fortov, M. Thoma, and O. Novitskii, Dust density waves in a dc flowing complex plasma with discharge polarity reversal, *Phys. Plasmas* **25**, 083705 (2018).
- [40] V. Yaroshenko, S. Khrapak, M. Pustyl'nik, H. M. Thomas, S. Jaiswal, A. Lipaev, A. Usachev, O. Petrov, and V. Fortov, Excitation of low-frequency dust density waves in flowing complex plasmas, *Phys. Plasmas* **26**, 053702 (2019).
- [41] D. I. Zhukhovitskii, Ionization equation of state for the dusty plasma including the effect of ion-Atom collisions, *Phys. Plasmas* **26**, 063702 (2019).
- [42] J. H. Jeans, I. the stability of a spherical nebula, *Philos. Trans. R. Soc. Lond. A* **199**, 1 (1902).
- [43] J. A. Peacock, *Cosmological Physics* (Cambridge University Press, Cambridge, England, 1999), chap. 15, p. 682.
- [44] Y. B. Zel'dovich, Gravitational instability: An approximate theory for large density perturbations., *Astron. Astrophys.* **5**, 84 (1970).
- [45] L. Hartmann, *Accretion Processes in Star Formation* (Cambridge University Press, Cambridge, England, 2000), Vol. 32, Chap. 2.2, p. 234.
- [46] A. Toomre, On the gravitational stability of a disk of stars, *Astrophys. J.* **139**, 1217 (1964).
- [47] D. Lynden-Bell, R. Wood, and A. Royal, The gravo-thermal catastrophe in isothermal spheres and the onset of red-giant structure for stellar systems, *Mon. Not. R. Astron. Soc.* **138**, 495 (1968).

- [48] R. B. Larson, Cloud fragmentation and stellar masses, *Mon. Not. R. Astron. Soc.* **214**, 379 (1985).
- [49] S. Bonazzola, J. Heyvaerts, E. Falgarone, M. Perault, and J. Puget, Jeans collapse in a turbulent medium, *Astron. Astrophys.* **172**, 293 (1987).
- [50] A. B. Romeo and N. Falstad, A simple and accurate approximation for the  $q$  stability parameter in multicomponent and realistically thick discs, *Mon. Not. R. Astron. Soc.* **433**, 1389 (2013).
- [51] K. Grisdale, O. Agertz, A. B. Romeo, F. Renaud, and J. I. Read, The impact of stellar feedback on the density and velocity structure of the interstellar medium, *Mon. Not. R. Astron. Soc.* **466**, 1093 (2017).
- [52] S. A. Khrapak and H. M. Thomas, Practical expressions for the internal energy and pressure of Yukawa fluids, *Phys. Rev. E* **91**, 023108 (2015).
- [53] A. P. Thompson, H. M. Aktulga, R. Berger, D. S. Bolintineanu, W. M. Brown, P. S. Crozier, P. J. in 't Veld, A. Kohlmeyer, S. G. Moore, T. D. Nguyen, R. Shan, M. J. Stevens, J. Tranchida, C. Trott, and S. J. Plimpton, LAMMPS—A flexible simulation tool for particle-based materials modeling at the atomic, meso, and continuum scales, *Comput. Phys. Commun.* **271**, 108171 (2022).
- [54] A. Zobnin, A. Usachev, O. Petrov, V. Fortov, M. Thoma, and M. Fink, Two-dimensional positive column structure with dust cloud: Experiment and nonlocal kinetic simulation, *Phys. Plasmas* **25**, 033702 (2018).
- [55] S. A. Khrapak, P. Tolias, S. Ratynskaia, M. Shaudhuri, A. Zobnin, A. Usachev, C. Rau, M. H. Thoma, O. F. Petrov, V. E. Fortov, and G. E. Morfill, Grain charging in an intermediately collisional plasma, *Europhys. Lett.* **97**, 35001 (2012).
- [56] V. E. Fortov, O. F. Petrov, A. D. Usachev, and A. V. Zobnin, Micron-sized particle-charge measurements in an inductive rf gas-discharge plasma using gravity-driven probe grains, *Phys. Rev. E* **70**, 046415 (2004).
- [57] H. Ellis, R. Pai, E. McDaniel, E. Mason, and L. Viehland, Transport properties of gaseous ions over a wide energy range, *At. Data Nucl. Data Tables* **17**, 177 (1976).